# Azimuthally polarized cathodoluminescence from InP nanowires

B. J. M. Brenny,[1] D. van Dam,[2] C. I. Osorio,[1] J. Gómez Rivas,[2,3] and A. Polman[1,a)]
[1]*Center for Nanophotonics, FOM Institute AMOLF, Science Park 104, 1098 XG Amsterdam, The Netherlands*
[2]*COBRA Research Institute, Eindhoven University of Technology, P.O. Box 513, 5600 MB Eindhoven, The Netherlands*
[3]*FOM Institute DIFFER, P.O. Box 6336, 5600 HH Eindhoven, The Netherlands*

(Received 9 September 2015; accepted 3 November 2015; published online 17 November 2015)

We determine the angle and polarization dependent emission from 1.75 μm and 2.50 μm long InP nanowires by using cathodoluminescence polarimetry. We excite the vertical wires using a 5 keV electron beam, and find that the 880 nm bandgap emission shows azimuthally polarized rings, with the number of rings depending on the wire height. The data agree well with a model in which spontaneous emission from the wire emitted into the far field interferes with emission reflected off the substrate. From the model, the depth range from which the emission is generated is found to be up to 400 nm below the top surface of the wires, well beyond the extent of the primary electron cloud. This enables a probe of the carrier diffusion length in the InP nanowires. © *2015 AIP Publishing LLC*.
[http://dx.doi.org/10.1063/1.4935798]

The research field of semiconductor nanowires has grown tremendously in the last two decades, due to the applications in optoelectronic devices, such as light-emitting diodes,[1,2] lasers,[3] photovoltaics,[4,5] photodetectors,[6] and more. The electrical properties of nanowires as well as their optical properties, such as the directionality and polarization of emitted radiation,[6–11] can be tuned by controlling the morphology, size, crystallinity, composition, and inclusions or junctions.[12–16] Among the nanowire materials, indium phosphide (InP) has a bandgap well-suited for photovoltaic applications, long carrier lifetime, and low surface recombination velocity.[17]

The light emission properties of semiconductor nanowires have mostly been studied using optical excitation techniques, which are limited in spatial resolution and therefore cannot access all details of the nanoscale emission mechanisms. Cathodoluminescence (CL) spectroscopy is an alternative technique that uses an electron beam as an excitation source, providing high excitation resolution and accessing a broad range of material transitions and defects.[18] Spatially resolved CL has shown that very thin (~20 nm diameter) InP nanowires exhibit polarized emission.[19] However, the angular distribution of the emitted light, which is crucial for many applications, is not resolved so far.

In this letter, we characterize the angle- and polarization-dependent emission from InP nanowires by using angle-resolved cathodoluminescence imaging polarimetry.[20] Previous studies of the directionality and polarization of semiconductor nanowires have focused on wires with high-aspect-ratio dimensions, whose behavior is dominated by waveguide modes.[7,10,11,21] In contrast, here we will examine low-aspect-ratio wires. We find that the angular emission from these short wires is dominated by azimuthally polarized rings that are not related to waveguide modes, and demonstrate that the emission and the number of rings are directly related to the wire height. The measurements are well-reproduced by a point dipole scattering and interference model and provide a measure for the carrier diffusion length in the wires.

We measured undoped InP nanowires grown vertically on an InP ⟨100⟩ substrate by a combination of vapor-liquid-solid (VLS) and vapor-solid (VS) methods.[11] Wires with an initial length of 8 μm were mechanically broken, resulting in wires 1.75±0.05 μm (NW1) and 2.50±0.05 μm (NW2) in length. Figures 1(a) and 1(b) show SEM images for both nanowires, taken for a tilt angle of 55°. We note that both wires are tapered in shape due to the growth process of the

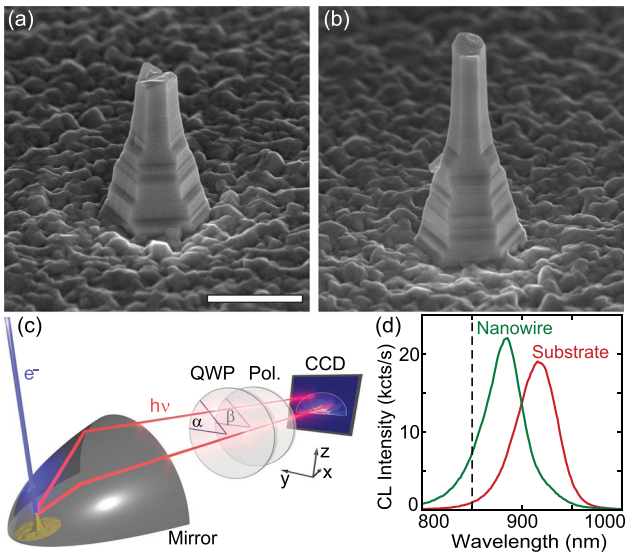


FIG. 1. Scanning electron micrographs of the InP nanowires NW1 (a) and NW2 (b), measured at a tilt angle of 55° (scale bar is 1 μm for horizontal dimensions and 1.2 μm for vertical dimensions). NW1 is 1.75 μm tall and 450 nm wide at the top; NW2 is 2.50 μm tall and 350 nm wide at the top; both wires are clearly tapered. (c) Schematic overview of the cathodoluminescence polarimetry setup. The electron beam excites the nanowires, and the emitted radiation is collected by a parabolic mirror and sent through a quarter-wave plate (QWP) and linear polarizer. Bandpass filters can be used to select a certain wavelength range and the resulting beam profile is measured by the CCD camera. (d) Measured CL emission spectra of NW2 (green) and substrate (red). The spectrum of NW1 (not shown) does not differ noticeably from that of NW2. The black dashed line at $\lambda_0 = 850$ nm indicates the transmittance maximum of the 40 nm bandwidth bandpass filter used for the angular measurements.

a)Electronic mail: polman@amolf.nl

 

base. NW1 and NW2 are 450 and 350 nm wide at the top, respectively, and are both 1.3 μm wide at the bottom of the base. This tapering will cause waveguide modes, which can play a role in short wires as well,[22] to be ill-defined.

The spectra and polarization-resolved angular emission patterns of the wires were measured using angle-resolved cathodoluminescence imaging spectroscopy and polarimetry. The emission resulting from exciting the wires with an electron beam from an SEM (5 keV, beam current ~0.4 nA) is collected by an aluminium parabolic mirror and directed to an optical setup. We can measure either the spectrum using a liquid-nitrogen-cooled back-illuminated silicon CCD array (Princeton Instruments Spec-10 100B) or the angular emission profile using a Peltier-cooled back-illuminated 2D silicon CCD array (Princeton Instruments PIXIS 1024B).[23,24] The angular imaging mode, shown schematically in Figure 1(c), includes a quarter-wave plate (QWP) and a linear polarizer (Pol.). These allow us to determine the Stokes parameters and therefore the polarization of the emitted radiation, including all electric field components.[25] To achieve this, we measure the intensities transmitted by six different combinations of QWP and polarizer positions (horizontal, vertical, 45°, 135°, right- and left-handed circular) and fully take into account the geometrical and polarization dependent effect of the parabolic mirror on the measured emission.[20]

The CL spectra of the InP nanowires peak at $\lambda_0 = 880$ nm, while the spectrum of the InP substrate is centered at $\lambda_0 = 920$ nm, as we show in Figure 1(d). This blueshift in the emission spectrum is due to a difference in crystal structure between the wires (mixed wurtzite–zinc blende) and the substrate (zinc blende).[11] The spectral shape of the nanowire spectrum indicates that the signal from the substrate is minimal for this measurement. This is due to the relatively shallow penetration depth of the 5 keV electrons, as shown in Figure 2(a), which displays the superimposed trajectories of $10^4$ electrons hitting the center of a 350 nm diameter InP wire, calculated using the Monte Carlo based software Casino.[26] The full interaction volume covers the entire diameter of the wire and reaches a depth of ~250 nm, generating electron-hole pairs in this region until the electrons fully relax. The large majority of excitations will take place in the first 200 nm, however, as shown by the dense region in Figure 2(a). The energy of the incident electrons decreases as they move further into the material, reducing the energy of the carriers that can be excited.

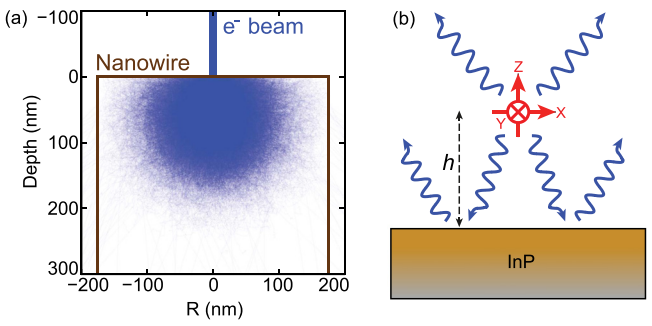


FIG. 2. (a) Monte Carlo simulation of $10^4$ electrons with 5 keV energy impinging the middle of an InP nanowire, using Casino.[26] All the electron trajectories are shown as superimposed partially transparent lines forming a blue cloud, indicating the interaction density and volume of the primary electrons with the wire. (b) Schematic of the dipole calculation. Separate X, Y, and Z oriented dipoles are placed in vacuum at a height $h$ above an InP surface. The direct emission interferes with light reflected off the substrate, and the calculation produces the resulting far field radiation patterns for all field components. The field intensities for the three orthogonal dipoles are incoherently added to simulate the behavior of randomly oriented dipoles.

The angular emission patterns of the wires exhibit a series of rings, as we show in Figures 3(a)–3(d), which display the measured angular emission patterns at $\lambda_0 = 850$ nm as a function of azimuthal ($\varphi$) and zenithal ($\theta$) angles. The dark blue regions in the measurement correspond to the angles at which no light is collected by the mirror. Figure 3(a) shows the total intensity ($I_{tot}$) for NW1, while Figures 3(b) and 3(c) compare the intensity of the radially polarized field component ($I_\theta$) with that of the azimuthally polarized field component ($I_\varphi$) for NW1. Figure 3(d) shows $I_\varphi$ for NW2. These figures show that the emission is dominated by azimuthally polarized rings and that the taller NW2 exhibits more rings than NW1. The intensity trends are similar to those in previous work on the angular emission profiles of plasmonic nanoantennas, which, for a fixed wavelength, exhibit an increasing number of rings for increasing antenna height.[27] The polarization was not resolved in this case however.

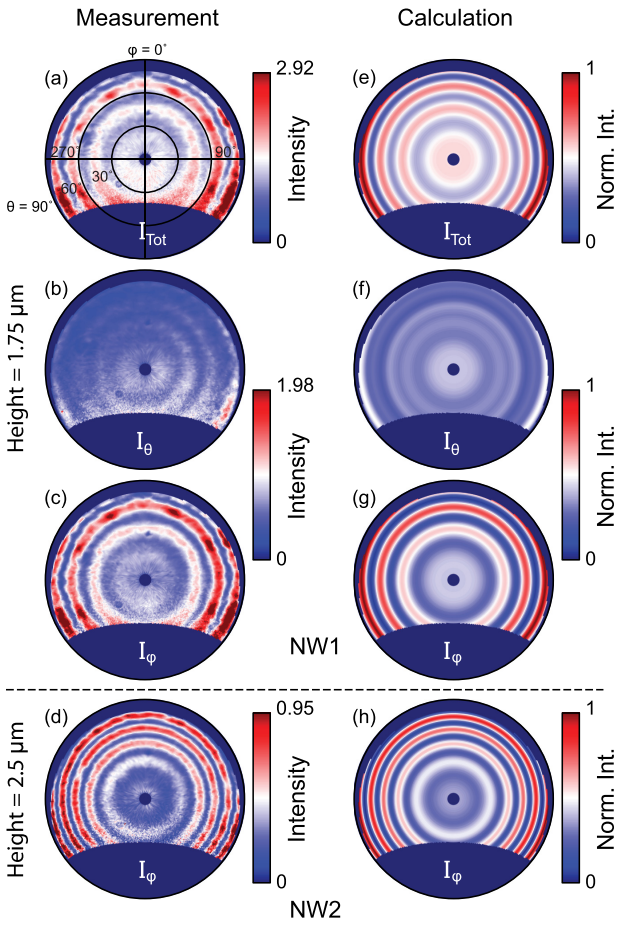


FIG. 3. Measured [(a)–(d)] and calculated [(e)–(h)] angular CL polarimetry emission intensities at $\lambda_0 = 850$ nm. The patterns were measured for central excitation of the nanowire, and the calculations averaged over a range of heights (65–415 nm below the surface, in steps of 10 nm, for both wires). (a) and (e) show the total intensity $I_{tot}$, (b) and (f) the radially polarized intensity $I_\theta$, and (c) and (g) the azimuthally polarized intensity $I_\varphi$, all for NW1. (d) and (h) show $I_\varphi$ for NW2. The $\theta$ and $\varphi$ polarized intensities for NW1 are shown on the same color scale. The calculations have been normalized to 1, while the measured intensities are given in $10^5$ counts $sr^{-1}$ $s^{-1}$.

In order to analyze the emission patterns, we model the spontaneous emission of the wires as an incoherent sum of point dipoles radiating in free space above a substrate, as shown schematically in Figure 2(b). We implement the Green's function formalism and asymptotic far field approximations from Ref. 28 as they are applied in Ref. 29; the measured far field radiation results from a superposition of the emission of the dipole and its image. We calculate the far field radiation patterns for separate X, Y, and Z oriented point dipoles at $\lambda_0 = 850$ nm (corresponding to the bandpass filter center wavelength) in vacuum, at a height $h$ above an InP substrate and incoherently add the intensities for different field components. We neglect the dielectric body of the nanowire itself, placing the dipoles in vacuum, in order to keep the model simple. We find this to be a valid approach as the emission only overlaps with the nanowire body for a small portion of angular space, namely, downwards where it will be guided into the substrate and absorbed. We use equal dipole amplitudes for the three orientations. The angular patterns result from the interference between the directly emitted radiation and the reflection from the substrate, and are therefore sensitive to the dipole height. The overall behavior is dominated by the X and Y dipoles, which combine to produce a strong azimuthal intensity distribution, while the Z dipole has a minor effect. To reflect the electron excitation volume, we have averaged the dipole positions over a range of heights, performing a calculation every 10 nm. Measurements and calculations agree best when using a height range of 350 nm, 65–415 nm below the top edge for both nanowires. The calculations accurately reproduce all major features of the measurements, such as the number of rings, zenithal emission angles, relative intensities, and polarization for both wires, as shown in Figures 3(e)–3(h). We find that the averaged calculation is quite sensitive to the chosen height range: moving the range up or down will shift the zenithal position of the rings, while increasing the range will decrease the amplitude of the intensity oscillations. A change of 10 nm or more already results in a noticeably larger difference with the measurement.

Examining $I_{tot}$ for NW1 (Figures 3(a) and 3(e)), we see in both measurement and calculation a region of higher intensity in the center and three rings of increasing intensity for increasing zenithal angle. For $I_\theta$ in NW1 (Figures 3(b) and 3(f)) the features are less pronounced but we notice a thin ring at the outer edge of both measurement and calculation. Figures 3(c) and 3(g) show the center disk and three rings of increasing intensity for $I_\varphi$, as for $I_{tot}$, confirming that the total emission is dominated by the azimuthally polarized contribution. We note that the measured data for $I_\theta$ and $I_\varphi$ are plotted with the same color scale. Finally, for $I_\varphi$ in NW2 (Figures 3(d) and 3(h)), five rings are observed, two more than those in NW1. Here too we find good agreement of both zenithal emission angles and relative intensities between measurement and calculation.

To quantitatively compare the measurements and calculations, we azimuthally average the data from Figure 3 (taking into account only the angles that are collected by the mirror) and show the result in Figure 4. The measured and calculated intensities are normalized to their corresponding total intensity. In Figure 4(a), we also show the calculation for a single dipole height for NW1 that most closely reproduces the

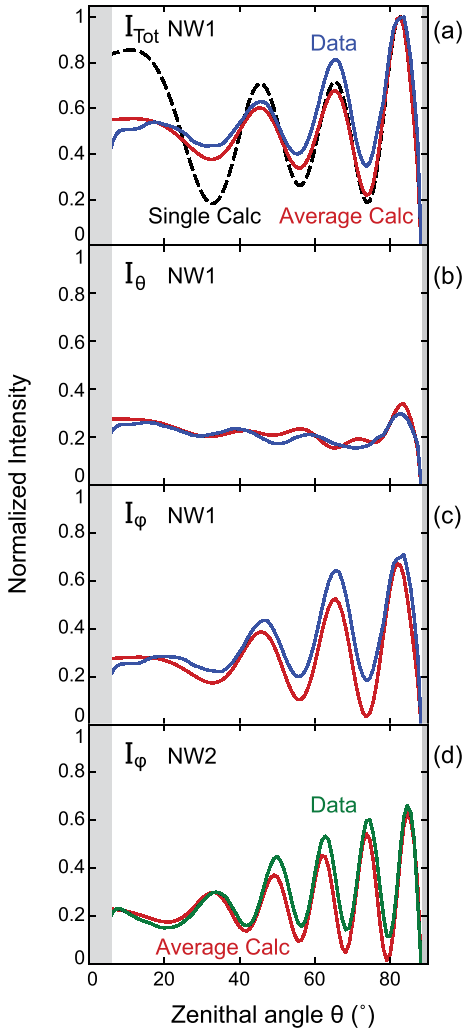


FIG. 4. Azimuthally averaged intensities from Figure 3, comparing the measurements (blue for NW1 and green for NW2) with the averaged calculations (red). All measured and calculated intensities are normalized to their respective total intensity. (a), (b), and (c) show $I_{tot}$, $I_\theta$, and $I_\varphi$, respectively, for NW1, while (d) shows $I_\varphi$ for NW2. In (a), the black dashed line indicates the calculation for a single height best matched to the measured data (1.52 μm). The gray areas represent the angular range not collected by the mirror.

intensity oscillations. We find for a single height that the oscillations at small values of $\theta$ have a much larger amplitude than in the data, while there is a very good match for the calculation that averages over a height range. The height range that best fits the data for both nanowires is larger than the extent of the primary electron cloud (~400 nm vs. ~200 nm below the top edge of the wires). It is known that carrier diffusion and photon recycling can enlarge the volume of light emission.[30] Carrier diffusion lengths of 160 nm have been measured in doped InP nanowires,[31] and for our undoped wires a larger diffusion length, on the order of a few hundred nanometers, is expected. Rather than using a simple model in which the carrier generation and light emission is fixed over a depth range, one could take into account a depth profile of carrier diffusion and recombination in the wires. This will allow the CL polarimetry presented here to directly determine the carrier diffusion length. Due to the high sensitivity to height changes of our simple model, on the order of 10 nm, we expect that the diffusion length can be resolved with a similar precision. Measurements using a range of electron beam

energies, and thus penetration depths, could be used to study the diffusion more accurately.

The features of $I_\theta$ in Figure 4(b) are much less pronounced than those of $I_\varphi$ in Figure 4(c), but in both cases there is very good agreement of the oscillations and the relative intensities, which is also the case for $I_\varphi$ for NW2 in Figure 4(d). A similar background signal is observed for both polarizations $I_\theta$ and $I_\varphi$, indicating that the emission also contains an unpolarized contribution.

In conclusion, we have demonstrated that InP nanowires, excited by a 5 keV electron beam at their top, display very distinctive angular emission rings that are strongly azimuthally polarized and dependent on wire height. The radiation is not dominated by the intrinsic angular emission of the nanowire itself, due to the tapering and low-aspect-ratio, but by interference of the luminescence with the substrate reflection. A dipolar model that calculates the interference between the directly emitted light and light reflected off the substrate reproduces the measured data well. The luminescence originates from a several hundred nanometer wide range near the top of the wire. The depth range is the same for both wires and is larger than the primary electron cloud, providing a measure for carrier diffusion in the wires. The capability to resolve the spectral, angular, and polarization properties of nanoscale excitation processes shows the power of cathodoluminescence polarimetry as a technique to study the highly tunable optical and electrical properties of semiconducting nanostructures with features much smaller than the optical diffraction limit.

We acknowledge Femius Koenderink, Mark Knight, and Toon Coenen for fruitful discussions, and E.P.A.M. Bakkers (Eindhoven University of Technology) for providing the InP sample. This work is part of the "Stichting voor Fundamenteel Onderzoek der Materie (FOM)" as well as the Dutch technology foundation STW, which are financially supported by the "Nederlandse Organisatie voor Wetenschappelijk Onderzoek (NWO)" and the Dutch Ministry of Economic Affairs. It is also part of NanoNextNL, a nanotechnology program funded by the Dutch Ministry of Economic Affairs, part of an industrial partnership program between Philips and FOM, and is supported by the European Research Council (ERC). A.P. is co-founder and co-owner of Delmic BV, a startup company developing a commercial product based on the cathodoluminescence system that was used in this work.

[1]K. Haraguchi, T. Katsuyama, and K. Hiruma, J. Appl. Phys. **75**, 4220 (1994).
[2]C. P. T. Svensson, T. Mårtensson, J. Trägårdh, C. Larsson, M. Rask, D. Hessman, L. Samuelson, and J. Ohlsson, Nanotechnology **19**, 305201 (2008).
[3]M. H. Huang, S. Mao, H. Feick, H. Yan, Y. Wu, H. Kind, E. Weber, R. Russo, and P. Yang, Science **292**, 1897 (2001).
[4]J. Wallentin, N. Anttu, D. Asoli, M. Huffman, I. Åberg, M. H. Magnusson, G. Siefer, P. Fuss-Kailuweit, F. Dimroth, B. Witzigmann, H. Q. Xu, L. Samuelson, K. Deppert, and M. T. Borgström, Science **339**, 1057 (2013).
[5]Y. Cui, J. Wang, S. R. Plissard, A. Cavalli, T. T. T. Vu, R. P. J. van Veldhoven, L. Gao, M. Trainor, M. A. Verheijen, J. E. M. Haverkort, and E. P. A. M. Bakkers, Nano Lett. **13**, 4113 (2013).
[6]J. Wang, M. S. Gudiksen, X. Duan, Y. Cui, and C. M. Lieber, Science **293**, 1455 (2001).
[7]A. V. Maslov and C. Z. Ning, Opt. Lett. **29**, 572 (2004).
[8]A. V. Maslov, M. I. Bakunov, and C. Z. Ning, J. Appl. Phys. **99**, 024314 (2006).
[9]J. Motohisa, Y. Kohashi, and S. Maeda, Nano Lett. **14**, 3653 (2014).
[10]G. Grzela, R. Paniagua-Domínguez, T. Barten, Y. Fontana, J. A. Sánchez-Gil, and J. Gómez Rivas, Nano Lett. **12**, 5481 (2012).
[11]D. van Dam, D. R. Abujetas, R. Paniagua-Domínguez, J. A. Sánchez-Gil, E. P. A. M. Bakkers, J. E. M. Haverkort, and J. Gómez Rivas, Nano Lett. **15**, 4557 (2015).
[12]R. Yan, D. Gargas, and P. Yang, Nat. Photonics **3**, 569 (2009).
[13]X. Duan, Y. Huang, Y. Cui, J. Wang, and C. M. Lieber, Nature **409**, 66 (2001).
[14]M. S. Gudiksen, L. J. Lauhon, J. Wang, D. C. Smith, and C. M. Lieber, Nature **415**, 617 (2002).
[15]M. Björk, B. Ohlsson, T. Sass, A. Persson, C. Thelander, M. Magnusson, K. Deppert, L. Wallenberg, and L. Samuelson, Nano Lett. **2**, 87 (2002).
[16]J. Claudon, J. Bleuse, N. S. Malik, M. Bazin, P. Jaffrennou, N. Gregersen, C. Sauvan, P. Lalanne, and J.-M. Gérard, Nat. Photonics **4**, 174 (2010).
[17]H. J. Joyce, C. J. Docherty, Q. Gao, H. H. Tan, C. Jagadish, J. Lloyd-Hughes, L. M. Herz, and M. B. Johnston, Nanotechnology **24**, 214006 (2013).
[18]D. Spirkoska, J. Arbiol, A. Gustafsson, S. Conesa-Boj, F. Glas, I. Zardo, M. Heigoldt, M. Gass, A. Bleloch, S. Estrade, M. Kaniber, J. Rossler, F. Peiro, J. Morante, G. Abstreiter, L. Samuelson, and A. Fontcuberta i Morral, Phys. Rev. B **80**, 245325 (2009).
[19]N. Yamamoto, S. Bhunia, and Y. Watanabe, Appl. Phys. Lett. **88**, 153106 (2006).
[20]C. I. Osorio, T. Coenen, B. J. M. Brenny, A. Polman, and A. F. Koenderink, e-print arXiv:1510.07976 [physics.optics].
[21]J. Claudon, N. Gregersen, P. Lalanne, and J.-M. Gérard, ChemPhysChem **14**, 2393 (2013).
[22]D. J. Traviss, M. K. Schmidt, J. Aizpurua, and O. L. Muskens, Opt. Express **23**, 22771 (2015).
[23]T. Coenen, E. J. R. Vesseur, A. Polman, and A. F. Koenderink, Nano Lett. **11**, 3779 (2011).
[24]T. Coenen, E. J. R. Vesseur, and A. Polman, Appl. Phys. Lett. **99**, 143103 (2011).
[25]M. Born and E. Wolf, *Principles of Optics: Electromagnetic Theory of Propagation, Interference and Diffraction of Light*, 7th ed. (Cambridge University Press, 1997).
[26]H. Demers, N. Poirier-Demers, A. R. Couture, D. Joly, M. Guilmain, N. de Jonge, and D. Drouin, Scanning **33**, 135 (2011).
[27]H. Acar, T. Coenen, A. Polman, and L. Kuipers, ACS Nano **6**, 8226 (2012).
[28]L. Novotny and B. Hecht, *Principles of Nano-Optics* (Cambridge University Press, 2006).
[29]F. Bernal Arango, A. Kwadrin, and A. F. Koenderink, ACS Nano **6**, 10156 (2012).
[30]N. M. Haegel, T. J. Mills, M. Talmadge, C. Scandrett, C. L. Frenzen, H. Yoon, C. M. Fetzer, and R. R. King, J. Appl. Phys. **105**, 023711 (2009).
[31]J. Wallentin, P. Wickert, M. Ek, A. Gustafsson, L. R. Wallenberg, M. H. Magnusson, L. Samuelson, K. Deppert, and M. T. Borgström, Appl. Phys. Lett. **99**, 253105 (2011).